Three-dimensional numerical simulation of blood flow in two coronary stent

F. Gori[a,b] and A. Boghi[a]

[a] *Department of Mechanical Engineering, University of Rome "Tor Vergata", Via del Politecnico 1, 00133 Roma, Italy.*

[b] *Corresponding author*

The aim of the present study is to carry out Computational Fluid Dynamics simulations in a realistic three dimensional geometry of two stent under physiological conditions. The two stent, similar to real coronary ones, are both made of 12 rings but are differing as far as the position of the struts is concerned. One type has parallel-connectors and the other transverse-ones. The artery is modeled as rigid cylinder and the fluid is assumed as incompressible Newtonian fluid in laminar flow with the average physical properties of blood. The commercial computational fluid dynamic code FLUENT is used with the mesh made of non-uniform tetrahedrons. The mesh independence is proved using the steady state results of the wall shear stress. The parameters correlated to neo-intimal hyperplasia, such as wall shear stress, magnitude of wall shear stress gradient, and oscillatory shear index, are investigated. Time variation of the parameters is investigated with the conclusion that the stent with parallel-connectors has a better fluid dynamic behavior.

Key index words: Coronary Stent; Blood Flow; Computational Fluid Dynamics.

1. INTRODUCTION

Atherosclerosis is one of the most common causes of death in the Western World. Stent is commonly used to restore blood flow in patients with severe coronary artery disease. Local hemodynamic variables, depending on stent geometry, have an important role in restenosis. The new drug eluting stent reduces significantly the percentage of restenosis (Morice *et al.* 2002; Moses *et al.* 2003; Schampaert *et al.* 2004; Schofer *et al.* 2003), also if the percent of restenosis in the long term may be similar to the classic one (Palmaz 2004; Virmani 2004) and the restenosis rates may be similar to the bare metal stent (Finn *et al.* 2005; Virmani *et al.* 2004). The new drug eluting stent does not help in healing the intima damaged by prior vascular disease or stent implantation procedure. These stent are not applicable to all patient populations and locations within the arterial vasculature (Farb *et al.* 2000) and cannot supplant the bare metal stent and avoid the fluid dynamics problems in device designing. Local hemodynamic variables, as wall shear stress, have an important

role in the restenosis and are dependent on stent geometry (Ku *et al.* 1985; Malek *et al.* 1999; Ku 1997).

Previous two-dimensional (2D) computational fluid dynamics (CFD) studies used simple stent geometry. Berry *et al.* (2000) investigated the influence of mesh dimension on the flow, suggesting that a small mesh can disturb the flow more than a big one. Lanoye *et al.* (2006) characterized the effect of the strut section, showing the round strut section disturbs the flow at a small extent. Seo *et al.* (2005) investigated the influence of the stent design near the curvatures, providing an understanding of the flow in the vicinity of the stent and suggesting strategies for the design optimization in order to minimize flow disturbance.

Few three-dimensional (3D) CFD studies have been carried out on stented arteries. LaDisa *et al.* (2002, 2003, 2004, 2005, 2005, 2006) characterized the stent design, and geometrical parameters as width, thickness and angle with the flow direction of the struts. He *et al.* (2005) studied realistic strut geometry, considering three geometric parameters of the struts and demonstrating the stent design is crucial in determining the fluid flow in an artery. Duraiswamy *et al.* (2008) provided a physiologic assessment on the effects of stent geometry on platelet deposition by using actual stent. Three-Dimensional Computational Fluid Dynamic models of the stent provided flow data explaining localized platelet deposition and identifying the regions of deposition. The localized platelet deposition is dependent on flow convection, suggesting that arterial reaction to stent can be modulated in part by altering the hemo-dynamics associated to stent design.

The goal of the present study is to reconstruct a realistic 3D geometry of a coronary stent in order to carry out CFD simulations in physiological conditions. A comparison is carried out between two reconstructed stent, made of 12 rings and similar to the real coronary ones. The two stent differ only by the position of the struts, the first type is with parallel-connectors and the second one with transverse-connectors. The artery is modeled as rigid cylinder and the fluid is an incompressible Newtonian fluid in laminar flow with the average physical properties of blood.

2. GEOMETRY

A real 3D geometry of a coronary stent, made of sequential rings and connected with longitudinal flexible connectors, is considered. Two different connections are investigated: regular peak to peak and mid-strut to mid-strut. The first type of stent is with parallel-connectors and the second one with transverse-connectors, (Stoeckel *et al.* 2002), similarly to the real coronary stent. In the rest of the paper the stent with parallel-connectors is named S1, and the one with transverse-connectors as S2. The software GAMBIT is used for reconstruction and mesh generation. The two complete reconstructed stent are shown in Figure 1a. Only a portion of the stent, 60° of the cylinder,

as shown in Fig. 1b, is investigated because of symmetry. Each reconstructed stent is made of 12 rings, artery diameter is 2.6 mm, with a width of 0.1 mm and total length of 27.6 mm, in agreement to a stented coronary artery (LaDisa *et al.* 2002) and a real coronary stent (Kastrati *et al.* 2001). The mesh used is made of non-uniform tetrahedrons having a minimum volume of $5.38 \cdot 10^{-16}$ m^3 and a maximum one of $4.82 \cdot 10^{-13}$ m^3, as shown in Figure 2.

3. GOVERNING EQUATIONS

The blood is assumed as incompressible Newtonian fluid in laminar flow with the average properties of blood, i.e. ρ = 1,060 kg m^{-3}, and μ=0.003333 kg·m^{-1} s^{-1}. The conservation equations of mass and momentum are respectively:

$$\nabla \cdot \vec{v} = 0 \tag{1}$$

and

$$\rho \frac{D\vec{v}}{Dt} = -\nabla p + \mu \nabla^2 \vec{v} \tag{2}$$

Equations (1-2) are solved with the following boundary conditions: no slip on artery and stented walls, prescribed blood flow (constant or physiologic waveform) on the inlet and constant pressure on the outlet. The commercial computational fluid dynamic code FLUENT is used to carry out simulations in steady and unsteady states.

In unsteady state the physiological waveform of mass flux, measured by LaDisa *et al.* (2002) in the proximal portion of a left anterior canine descending coronary artery, is employed, as shown in Figure 3. The artery diameter is the same as the diameter of the reconstructed artery. The waveform of Figure 3, sum of sinusoidal functions, is used as UDF input in the code FLUENT. In steady state the mean value of this waveform is used, 104.85 kg m^{-2} s^{-1}. Simulations are carried out using a Core 2 Duo 2.2 GHz Intel Mobile Centrino with 2 GByte of RAM, running LINUX. The residuals values for mass and three velocity components, after 1000 iterations, are lower than 10^{-6} for all cases. In unsteady state the total investigated time (0.8 s) is split into 800 time steps, and 20 iterations are done for each period.

4. FLUID DYNAMICS PARAMETERS

The most important fluid dynamic parameter, according to the literature, is the wall shear stress (WSS), defined, in cylindrical coordinates, by

$$WSS = \mu \sqrt{\left[\left(\frac{1}{r} \frac{\partial v_r}{\partial \vartheta} + \frac{\partial v_\vartheta}{\partial r} - \frac{v_\vartheta}{r} \right)^2 + \left(\frac{\partial v_r}{\partial z} + \frac{\partial v_z}{\partial r} \right)^2 \right]}_{wall} \tag{3}$$

where v_r and v_θ are the r and θ components of the velocity, respectively. According to previous studies of the literature a low wall shear stress is below 0.5 Pa. Another important parameter used in

literature is the spatial wall shear stress gradient (DePaola *et al.* 1992), WSSG, defined, in cylindrical coordinates, by

$$WSSG = \begin{bmatrix} \frac{\partial WSS_r}{\partial r} & \frac{1}{r}\frac{\partial WSS_r}{\partial \vartheta} - \frac{WSS_\vartheta}{r} & \frac{\partial WSS_r}{\partial z} \\ \frac{\partial WSS_\vartheta}{\partial r} & \frac{1}{r}\frac{\partial WSS_\vartheta}{\partial \vartheta} - \frac{WSS_r}{r} & \frac{\partial WSS_\vartheta}{\partial z} \\ \frac{\partial WSS_z}{\partial r} & \frac{1}{r}\frac{\partial WSS_z}{\partial \vartheta} & \frac{\partial WSS_z}{\partial z} \end{bmatrix} \quad (4)$$

where WSS_r and WSS_θ are the r and θ components of the WSS, respectively. The modulus of this matrix is defined as:

$$MGS = \sqrt{\sum_{i=1}^{3}\sum_{j=1}^{3}\left(WSSG_{ij}\right)^2} \quad (5)$$

High values of magnitude of wall shear stress gradient, MGS are related to neo-intimal hyperplasia.

The oscillatory shear index (OSI) is defined as, [27],

$$OSI = \frac{1}{2}\left(1 - \frac{\int_0^T WSS_z\, dt}{\int_0^T \left\| WSS_z \right\| dt}\right) \quad (6)$$

where T is the period. OSI is investigated to measure the degree of deviation of the wall shear stress from its average direction during pulsatile flow.

5. RESULTS

5.1 Mesh

Figure 4 presents the results of three simulations with different meshes, in order to show the spatial mesh independence of WSS, according to the proposal of Prakash *et al.* (2001). Figure 4 reports the average WSS for three different meshes, with about 765,000, 1,900,000 and 3,100,000 cells for both stent. Concerning the S2 stent the minimum and maximum percentage difference between 765,000 and 1,900,000 cells are about 3.46% and 0.29% while the minimum and maximum percentage difference between 1,900,000 and 3,100,000 cells are about 2.26% and 0.13%. Concerning the S1 stent the minimum and maximum percentage difference between 765,000 and 1,900,000 cells are about 2.33% and 0.03% while the minimum and maximum percentage difference between 1,900,000 and 3,100,000 cells are about 1.76% and 0.13%. The WSS distributions are enough close among the three simulations with the conclusion that a mesh with 765,000 cells is a good compromise.

5.2 Steady state simulations

The average WSS is reported versus the axial length in Figure 5, where the average is relative only to the endothelium, not to the stent. This is the reason of the low values of WSS. Figure 5 shows a repeating pattern of WSS being a periodic function which presents intermittent

localized lower oscillations, due to the protrusion of the curved shape struts. WSS is greater in the S1 stent, as compared to the S2 one, due to the skewing of velocity profile, caused by the transverse struts of the S2 stent. The lowest values of WSS are due to the presence of stagnation regions, while highest values are in the center of the cell, where velocity vectors are parallel to the wall. The differences between two WSS profiles are small, e.g. of the order of 0.1 Pa. Moreover, the spatial oscillations of WSS are low in each single stent, e.g. of the order of 0.35Pa.

Distributions of WSS and MGS are presented in Figure 6 for each stent. Stagnation zones occurred around and between stent struts, generating lower WSS in both stent while, far from the struts, regions with higher WSS are observed. Velocity changes direction due to the stent, but, because of the small stent thickness, the occurring vortex is very small and can promote proteins deposition. The nominal diameter of the vessel is reduced on the stent surface, producing converging streamlines and higher WSS, while, after the stent struts, higher nominal diameters are present and the diverging streamlines produce lower WSS. The diverging effect is enough low to disappear in one strut diameter and to give higher WSS at the center of each repeating stent unit. Higher WSS is present on the stent surface, not shown in Figure 6 because the main interest is the endothelium effect. Lower WSS are present around the stent struts in the region of transition between vessel and stent. The conclusion is a large difference between WSS in a small region, causing high MGS. Physiological values of WSS span between 0.5 Pa and 0.8 – 1 Pa (Ku *et al.* 1985; Malek *et al.* 1999). Low WSS values are strongly related to endothelial permeability and can promote neo-intimal hyperplasia, while values higher than 1 Pa seem to have no relation with neo-intimal hyperplasia. Steady state WSS of both stent shows that the regions of the vessel wall surrounding the stent have a uniform WSS distribution, with values lower than 0.5 Pa. No substantial difference is reported between the two stent but these areas have a larger extension in the S2 stent.

Steady state MGS are presented in Figure 7. MGS values on stent are less interesting because high values of MGS are related to restenosis but their range has not been established yet. Regions with higher MGS are in the zone of transition between vessel and stent, while lower MGS are present between the angled struts, where is present a region with uniform WSS, due to stagnation region. Regions opposing the mean flow are highly dangerous because hyperplasia can develop here. The S2 stent presents higher values of MGS than the S1 one.

5.3 Unsteady state simulations

Unsteady state simulations, performed during two periods of the cardiac cycle, show large variations of WSS and MGS with time. Figure 8 reports the time variation of the average WSS over

the endothelium, showing that average WSS of the two stent has a similar pattern but higher values are present in the S1 stent. Moreover, the differences are more significant at the systolic peak, due to stent geometry. In the S2 stent, struts of adjacent cells become parallel in proximity of the intersecting points of the struts, where the flow is trapped and WSS is quasi time-independent. The absence of these zones in the S1 stent makes the WSS increase with the flow rate more evidently leading to the differences visible in Figure 8.

Figure 9-10 present WSS and MGS patterns at six different times for S1 and S2 stent. WSS and MGS increase with the systolic wave because velocity increases with the pressure, but it must be null on the stent, due to no slip condition. Stagnation zones are present for all cardiac cycles, although their extension decreases with the increase of velocity. Areas adjacent to the stent struts present low WSS values for all cardiac cycles because of stagnation regions. WSS has large variations close to the vessel wall where the velocity is free to increase. Low MGS values are present on the vessel wall during the entire cardiac cycle. WSS increases on the vessel wall with values spanning between 0 and 2.5 Pa, while MGS spans in the range between 0 and 16,000 Pa/m.

MGS increases with the flow rate. Regions of high MGS are adjacent to the stent struts, except around the curved ones which surround the stagnation regions where uniform and low WSS can be noticed. Uniform values of WSS mean low MGS. A different pattern is observed on the others struts because of high WSS gradient, which increases during the flow rate, reaching a maximum on the edge of the curved struts. High increase of WSSG along the edge of the curved struts is produced, due to the strong redirection of the velocity profile, which is caused by angular struts changing WSS direction.

OSI results are presented in Figure 11, showing that the stent with S2 presents large regions with OSI greater than 0.5. Regions with non zero OSI are present between the handles of the struts and in the regions surrounding the points with discontinuity in the tangent. The stent with S2 has the highest curvature on the angular struts, connecting repeating stent unit, and its axis has a transverse direction which disturbs the flow and presents larger regions with non zero OSI. In the stent with S1 the axis of the connecting struts are parallel to the flow direction, and the angular struts are longer in the stent with S2, disturbing the flow of a similar amount. The OSI parameter, which gives additional information besides WSS and MGS, shows that large differences in the fluid dynamics of the two stent are present in unsteady state.

It is also possible to estimate the percent of critical intra strut areas, P, exposed to low WSS (< 0.5 Pa) during the cardiac cycle, defining

$$P = percArea(\%) = 100 \frac{\int_{vesel\_wall} \frac{1}{2}\left(1 - \left(\frac{WSS - 0.5}{\|WSS - 0.5\|}\right)\right) dA}{\int_{vesel\_wall} dA} \tag{7}$$

Figure 12 shows that the stent with S2 has lower values of percent critical intra strut area, P. The P value on the stented region, exposed to WSS smaller than 0.5 Pa, reduces as flow rate increases, reaching the minimum value at the point of the cardiac cycle corresponding to peak flow velocity. Since WSS increases with the velocity, the endothelium surface will be exposed averagely to higher WSS during the systole, decreasing the risk of developing neo-intimal hyperplasia.

6. DISCUSSION

The present work investigates two stent configurations called S1 and S2. Numerical simulations in the S2 stent show that the near-wall velocity vectors are misaligned with the flow direction, contributing to generate hazardous WSS and MGS distributions. Numerical simulations are carried out in order to answer to the question whether a parallel-connectors stent is preferable to a transverse-connectors one to reduce restenosis. The differences of the critical WSS values between the two stent are around 6.5%, while the percent of critical intra strut areas, P, increases of 4.2% in stent S2, but, more important, the great part of the stent region is subject to WSS which are lower than the critical value in both stent. The S1 stent seems slightly better from the fluid dynamics point of view than S2. The results presented here are valid only for the stent examined but the results may suggest that connecting the struts with connectors parallel to the mean flow can reduce the restenosis rate.

The parameters used to evaluate the stent suggest that S1 one is better. These conclusions are consistent with the physical intuition that optimal design should minimize changes in blood flow characteristics (LaDisa *et al.* 2005). Moreover, the results of the present paper seem to confirm the experimental observations of (Duraiswamy *et al.* 2008), where, among the stent studied, the Bx Velocity stent is similar to the present S2 stent. Indeed, it was shown in (Duraiswamy *et al.* 2008) that the nearly helically recirculating regions, near the connectors, exhibit complex fluid dynamics with more platelet deposition. The indicators employed in the present paper, for instance low WSS, high MGS and OSI, are in agreement to the predictions of the platelet deposition observed in (Duraiswamy *et al.* 2008).

The present numerical study has the following assumptions: i) the left anterior descending coronary artery, where the device is embedded, is not a straight cylinder, so, simulations could be function of the axial length because of the curved geometry of the artery; ii) simulations are not performed in a diseased artery; iii) simulations are performed on a rigid wall, which is different from the material of elastic artery; iv) initial conditions assumed on the blood flow are relative to proximal portion of left anterior canine descending coronary artery; v) blood is assumed as Newtonian fluid.

As far as the third limitation is concerned, the rigid wall should not affect significantly the results because studies on animals (LaDisa *et al.* 2003) assure that stent implantation reduces the vessel compliance to zero within the stented region (Ebeid *et al.* 2003) and wall deformability does not greatly alter the velocity field under normal conditions. Probably, the condition that could mainly affect the results is the fifth one because the waveform assumed in the simulations is relative to the left anterior canine descending coronary artery, found in literature, which may differ from a patient specific one. This waveform is assumed also because it has been employed in (LaDisa *et al.* 2002) as a valid boundary condition.

Despite the previous considerations it must be pointed out the potential clinical applicability of the current results, due to the growing interest in employing drug-eluting stent in order to reduce the percentage of restenosis. Local flow patterns, due to the presence of the stent, must be taken into account during stent design, in order to avoid values of fluid dynamics parameters involved in neo-intimal hyperplasia. An increasing number of evidences suggest that geometry and physical properties of a deployed stent may influence blood flow and alter WSS distributions after implantation, rendering certain areas of the vessel wall more susceptible to neo-intimal hyperplasia and restenosis (Virmani *et al.* 2004, 2004; LaDisa *et al.* 2005).

This is the reason of the investigation of physical parameters influencing the geometrical features that may enhance platelet and proteins deposition, and causing pathological conditions. The physical parameters promoters of neo-intimal hyperplasia are low WSS, high space and time WSSG, and geometrical features as number, width and thickness of strut to struts, stent-to-artery deployment diameter, and stent scaffolding. Assessment on the influence of fluid dynamics parameters and geometrical configuration has been carried out with computational fluid dynamics models (DePaola *et al.* 1992) and experimental studies (Benard *et al.* 2003), but *in vivo* testing is still lacking.

7. CONCLUSIONS

Two stent with different design, the first one with parallel-connectors, S1, and the second with transverse-connectors, S2, are investigated performing CFD simulations in steady and unsteady state. According to the literature, the parameters involved in the restenosis are WSS, MGS and OSI, because they are related to neo-intimal hyperplasia. Numerical simulations show the presence of regions close to the stent where WSS is lower than critical value, while, close to the stent elements opposing the flow, high MGS values are predicted. Unsteady simulations show the presence of large difference between instantaneous and mean values of WSS and MGS. Unsteady analysis suggests to use the parameter OSI, which shows the presence of regions with non zero values, located in regions surrounding the angular points of the stent. It is then possible to conclude

that the S2 stent has a better fluid dynamic behavior. These results may lead to the suggestion that the transverse connectors may increase the restenosis rate. Future investigations are required on different stent geometries involving parallel and transverse connectors. The evidence of the fluid dynamics parameters involved in restenosis suggests the importance of the hemodynamic behavior in the choice of a stent.

REFERENCES

Benard, N., Coisne, D., Donal, E. & Perrault, R. 2003 Experimental study of laminar blood flow through an artery treated by a stent implantation: characterization of intra-stent wall shear stress. *Journal of Biomechanics*. **36**, 991–998. (doi:10.1016/S0021-9290(03)00068-X)

Berry, J. L., Santamarina, A., Moore, J. E. Jr., Roychowdhury, S. & Routh, W. D. 2000 Experimental and computational flow evaluation of coronary stents. *Annuals of Biomedical Engineering*. **28(4)**, 386-98.

DePaola, N., Gimbrone, M. A. Jr., Davies, P. F. & Dewey C. F. 1992 Vascular endothelium responds to fluid shear stress gradients. *Arterioscler. Thromb.*; **12,** 1254-1257. ()

Duraiswamy, N., Cesar, J. M., Schoephoerster, R. T. & Moore, J. E. Jr. 2008 Effects of stent geometry on local flow dynamics and resulting platelet deposition in an *in vitro* model. *Biorheology*; **45**, 547–561. (doi:10.3233/BIR-2008-0497)

Ebeid M. R. Balloon expandable stents for coarctation of the aorta: review of current status and technical considerations. 2003 *Images in Pediatric Cardiology;* **15**: 25-41. (doi:10.1016/S0735-1097(97)00408-7)

Farb, A., Tang, A. L., Shroff, S., Sweet, W., Virmani, R. 2000 Neointimal responses 3 months after ^{32}P β-emitting stent placement. *International Journal of Radiation Oncology Biology Physics;* **48** (3): 889-98. (doi:10.1016/S0360-3016(00)00661-1)

Finn, A. V., Palacios, I. F., Kastrati, A., Gold, H. K. 2005 Drug-eluting stents for diabetes mellitus: a rush to judgment? *J. Am. Coll. Cardiol.;* **45**:479-483. (doi:10.1016/j.jacc.2004.10.060)

He, Y., Duraiswamy, N., Frank, A. O., Moore, J. E. Jr. 2005 Blood Flow in Stented Arteries: A Parametric Comparison of Strut Design Patterns in Three Dimensions. *Journal of Biomechanical Engineering*; **127**: 637-647. (doi:10.1115/1.1934122)

Kastrati, A., Mehilli, J., Dirschinger, J., Pache, J., Ulm, K., Schühlen, H., Seyfarth, M., Schmitt, C., Blasini, R., Neumann, F. J., Schömig, A. 2001 Restenosis after coronary placement of various stent types. *Am. J. Cardiol.;* **87**(1): 34-39. (doi:10.1016/S0002-9149(00)01268-6)

Ku, D.N., Giddens, D. P., Zarins, C. K., Glagov, S. 1985 Pulsatile flow and atherosclerosis in the human carotid bifurcation. Positive correlation between plaque location and low oscillating shear stress. *Arteriosclerosis;* **5**: 293-302.

Ku, D. N. 1997 Blood flow in arteries. *Ann. Rev. Fluid Mech.;* **29**: 399-434. (doi:10.1146/annurev.fluid.29.1.399)

LaDisa, J. F. Jr., Hettrick, D. A., Olson, L. E., Guler, I., Gross, E. R., Kress, T. T., Kersten, J. R., Warltier, D. C., Pagel, P. S. 2002 Coronary stent implantation alters coronary artery hemodynamics and wall shear stress during maximal vasodilation. *Journal of Applied Physiology;* **93**: 1939-1946. (doi:10.1152/japplphysiol.00544.2002)

LaDisa, J. F. Jr., Guler, I., Olson, L. E., Hettrick, D. A., Kersten, J. R., Warltier, D. C., Pagel, P. S. 2003 Three dimensional computational fluid dynamics modeling of alterations in coronary artery wall shear stress produced by stent implantation. *Annuals of Biomedical Engineering;* **31**: 972-980. (doi:10.1114/1.1588654)

LaDisa, J. F. Jr, Olson, L. E., Guler, I., Hettrick, D. A., Audi, S. H. 2004 Stent design properties and deployment ratio influence indexes of wall shear stress: a three dimensional computational fluid dynamics investigation within a normal artery. *Journal of Applied Physiology;* **97**(1): 424-30. (doi:10.1152/japplphysiol.01329.2003)

LaDisa, J. F. Jr., Olson, L. E., Hettrick, D. A., Warltier, D. C., Kersten, J. R. and Pagel, P. S. 2005 Axial stent strut angle influences wall shear stress after stent implantation: analysis using 3D computational fluid dynamics models of stent foreshortening. *BioMedical Engineering OnLine;* **4**: 59. (doi:10.1186/1475-925X-4-59)

LaDisa, J. F. Jr., Olson, L. E., Guler, I., Hettrick, D. A., Kersten, J. R., Warltier, D. C. and Pagel, P. S. 2005 Circumferential vascular deformation after stent implantation alters wall shear stress evaluated with time-dependent 3D computational fluid dynamics models. *Journal of Applied Physiology;* **98**: 947-957. (doi:10.1152/japplphysiol.00872.2004)

LaDisa, J. F. Jr., Olson, L. E., Hettrick, D. A., Warltier, D. C., Kersten, J., and Pagel, P. 2006 Alterations in regional vascular geometry produced by theoretical stent implantation influence distributions of wall shear stress: analysis of a curved coronary artery using 3D computational fluid dynamics modeling. *BioMedical Engineering OnLine;* **5**: 40. (doi:10.1186/1475-925X-5-40)

Lanoye, L., De Beule, M., Dewijngaert, C., Segers, P., Van Impe, R., and Verdonck, P. 2006 The influence of the strut section shape on the flow field in a newly stented right coronary artery. *The 56th National Congress of Theoretical and Applied Mechanics*, NCTAM.

Malek, A. M., Alper, S. L., and Izumo, S. 1999 Hemodynamic shear stress and its role in atherosclerosis. *JAMA;* **282**: 2035-2042.

Morice, M. C., Serruys, P. W., Sousa, J. E., Fajadet, J., Ban Hayashi, E., Perin, M., Colombo, A., Schuler, G., Barragan, P., Guagliumi, G., Molnàr, F., and Falotico, R. 2002 A randomized comparison of a sirolimus-eluting stent with a standard stent for coronary revascularization. *N. Eng. J. Med;* **346** (23): 1773-1780. (doi:10.1016/j.jacc.2005.10.078)

Moses, J. W., Leon, M. B., Popma, J. J., Fitzgerald, P. J., Holmes, D. R., O'Shaughnessy, C., Caputo, R. P., Kereiakes, D. J., Williams, D. O., Teirstein, P. S., Jaeger, J. L., Kuntz, R. E. 2003 Sirolimus-eluting stents versus standard stents in patients with stenosis in a native coronary artery. *N. Engl. J. Med.;* **349**(14): 1315-1323.

Palmaz, J.C. 2004 Intravascular stents in the last and the next 10 years. *J. Endovasc. Ther. Suppl.;* **2**, 200-206. (doi: 10.1583/04-1363.1)

Prakash, S., and Ethier, C. R. 2001 Requirements for Mesh Resolution in 3D Computational Hemodynamics. *Journal of Biomechanical Engineering;* **123**(2):134-44.

Schampaert, E., Cohen, E. A., and Schluter, M. 2004 The Canadian study of the sirolimus-eluting stent in the treatment of patients with long de novo lesions in small native coronary arteries (C-SIRIUS). *J. Am. Coll. Cardiol.;* **43**: 1110-1115. (doi:10.1016/j.jacc.2004.01.024)

Schofer, M., and Gershlick, A. H. 2003 Sirolimus-eluting stents for treatment of patients with long atherosclerotic lesions in small coronary arteries: double-bind, randomized controlled trial. *Lancet;* **362**: 1093-1099.

Seo, T., Schachter, L. G., and Barakat, A. I. 2005 Computational Study of Fluid Mechanical Disturbance Induced by Endovascular Stents. *Annals of Biomedical Engineering;* **33**(4), 444-456. (doi:10.1007/s10439-005-2499-y)

Stoeckel, D., Bonsignore, C., and Duda S. 2002 A survey of stent designs. *Min. Invas. Ther. & Allied Technol.;* **11**: 137-147. (doi:10.1080/136457002760273340)

Taylor, C. A., Hughes, T. J. R., and Zarins C.K. 1998 Finite Element Modeling of Three-Dimensional Pulsatile Flow in the Abdominal Aorta: Relevance to Atherosclerosis. *Annals of Biomedical Engineering*; **26**:975–987.

Virmani, R., Farb, A., Guagliumi, G., and Kolodgie F. D. 2004 Drug-eluting stents: caution and concerns for long-term outcome. *Coronary Artery Disease;* **15**:313-318.

Figure captions.

Figure 1 - Reconstructed geometries: (a) complete stent, S2 on the left and S1 on the right, (b) geometry used for numerical simulations.

Figure 2 - Mesh.

Figure 3 - Physiological inlet waveform of mass flux.

Figure 4 - WSS spatial distribution for different numbers of cells. S1 are on top and S2 on bottom.

Figure 5 - WSS on endothelium for S1 and S2 stent.

Figure 6 – Steady state distributions of WSS. S2 stent is on the left and S1 one on the right.

Figure 7 – Steady state MGS. S2 stent is on the left and S1 one on the right.

Figure 8 - WSS on endothelium for S1 stent and S2 one.

Figure 9 - WSS in unsteady state for S2 stent on the left and S1 one on the right.

Figure 10 – MGS in unsteady state for S2 stent on the left and S1 one on the right.

Figure 11 – OSI for S2 stent on the left and S1 one on the right.

Figure 12 – Critical percent critical intra strut area.

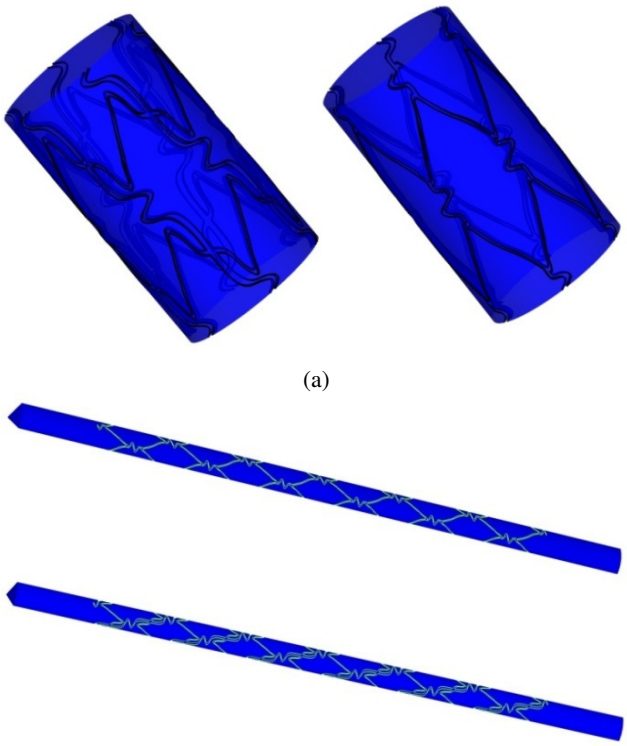

(a)

(b)

Figure 1 - Reconstructed geometries: (a) complete stent, S2 on the left and S1 on the right, (b) geometry used for numerical simulations.

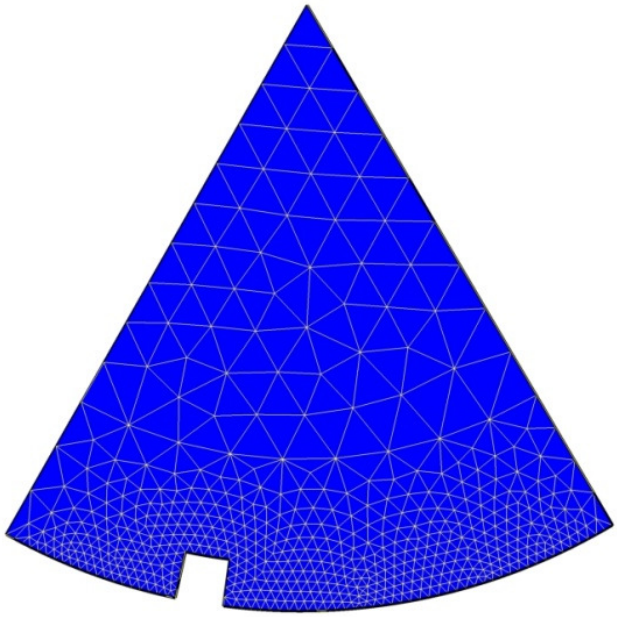

Figure 2 - Mesh.

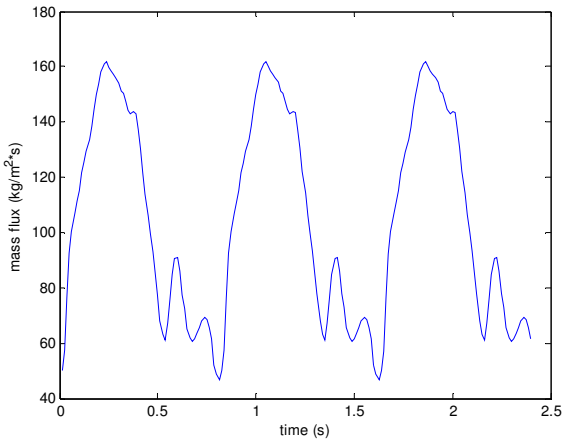

Figure 3 - Physiological inlet waveform of mass flux.

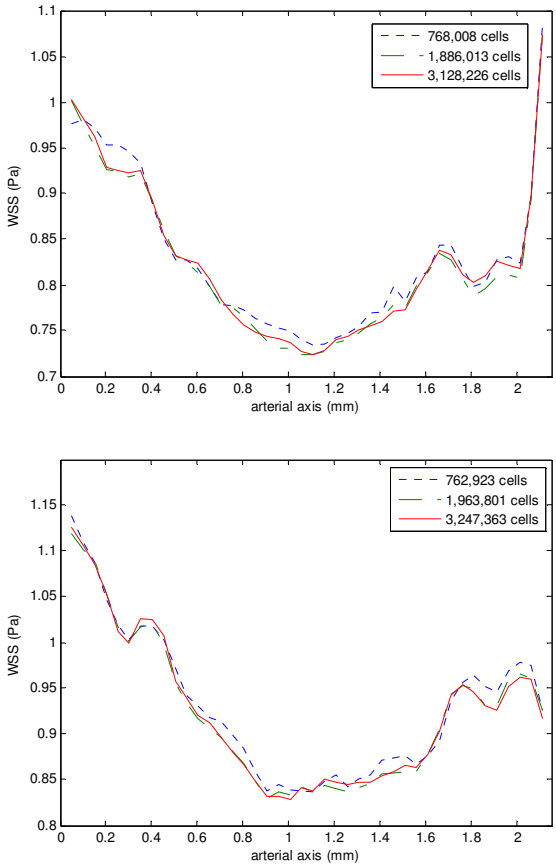

Figure 4 - WSS spatial distribution for different numbers of cells. S1 are on top and S2 on bottom.

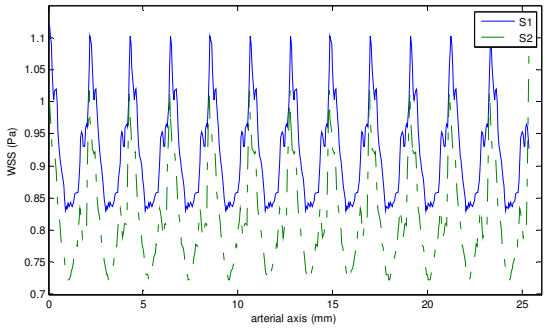

Figure 5 - WSS on endothelium for S1 and S2 stent.

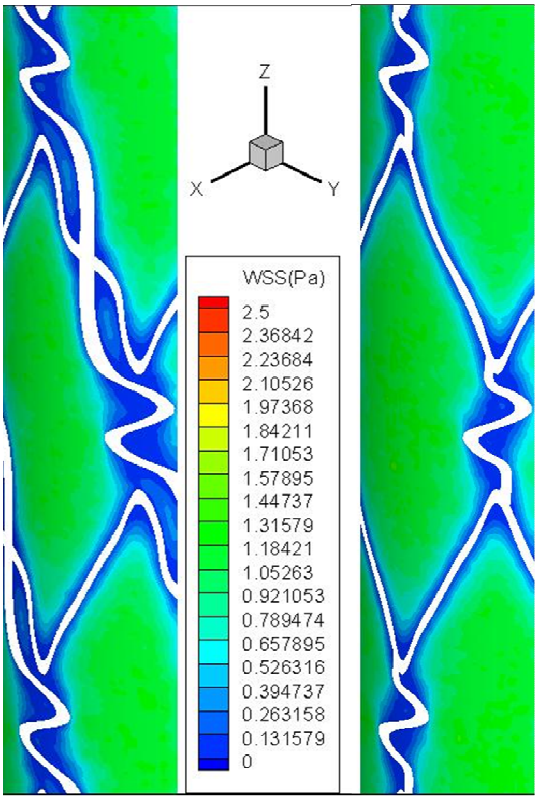

Figure 6 – Steady state distributions of WSS. S2 stent is on the left and S1 one on the right.

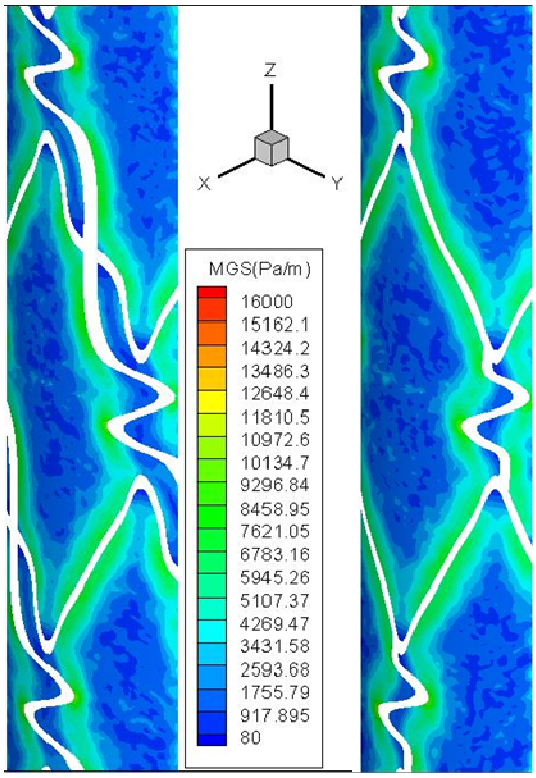

Figure 7 – Steady state MGS. S2 stent is on the left and S1 one on the right.

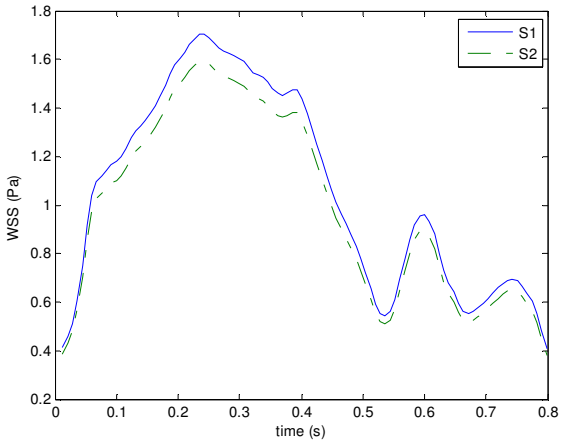

Figure 8 - WSS on endothelium for S1 stent and S2 one.

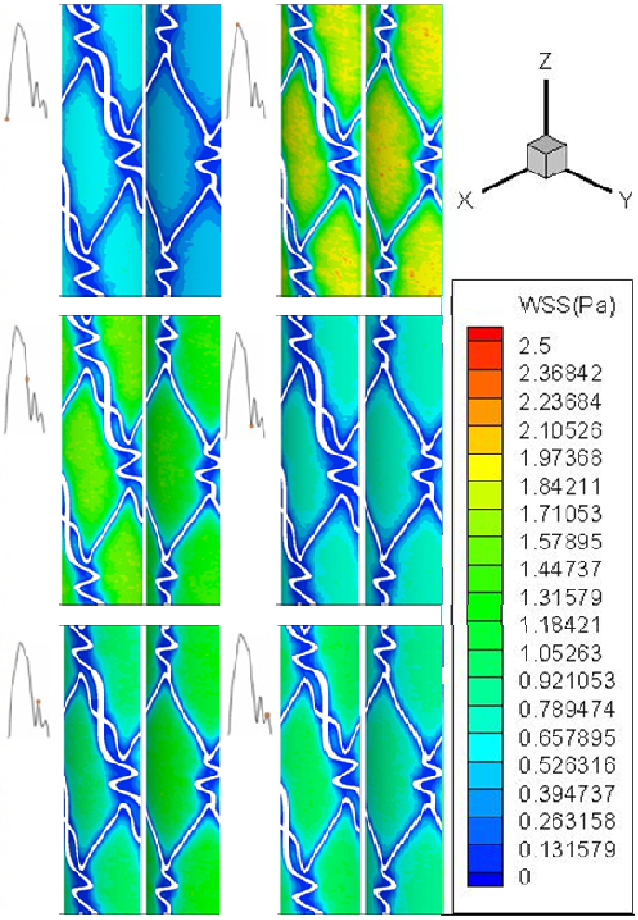

Figure 9 - WSS in unsteady state for S2 stent on the left and S1 one on the right.

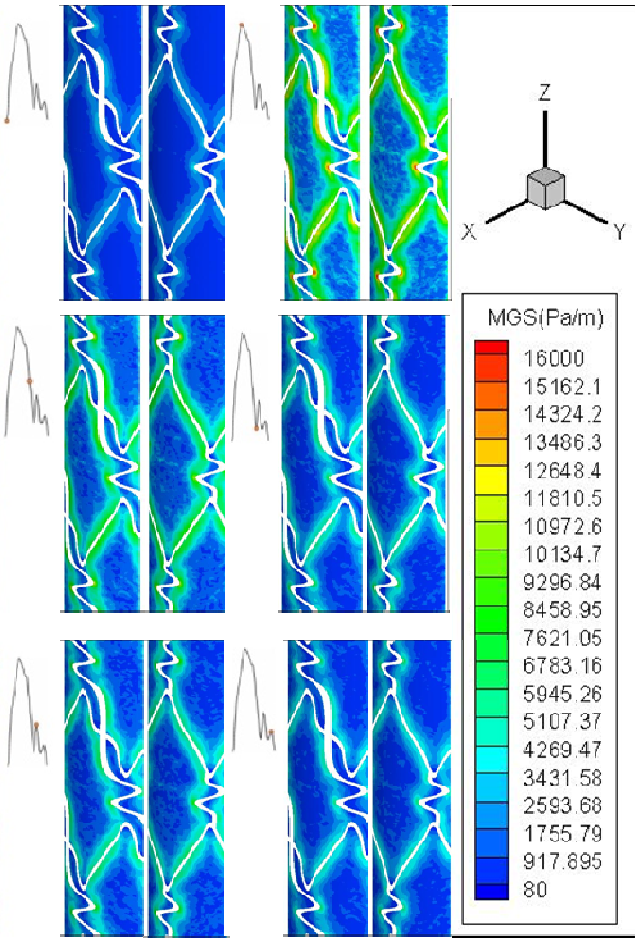

Figure 10 – MGS in unsteady state for S2 stent on the left and S1 one on the right.

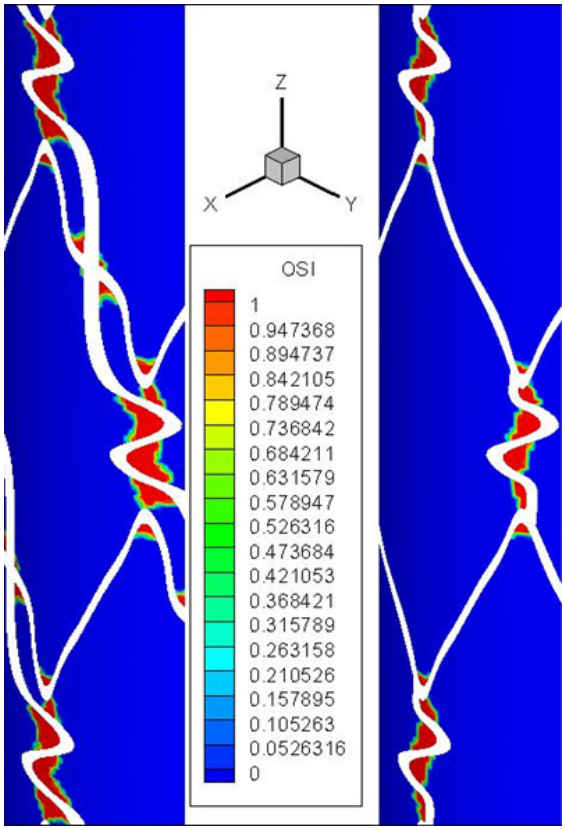

Figure 11 – OSI for S2 stent on the left and S1 one on the right

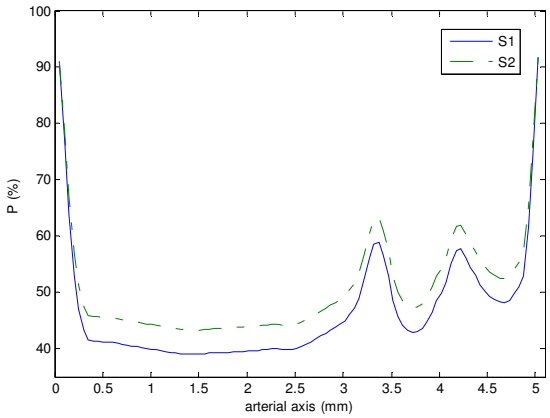

Figure 12 – Critical percent critical intra strut area.